

## Article

# Investigation of the Laser Material Interaction of Lithium Copper Foils Under Different Process Gases for All-Solid-State Batteries

Lars O. Schmidt \* , Houssin Wehbe , Sven Hartwig  and Maja W. Kandula

Institute of Joining and Welding, Technical University Braunschweig, 38106 Braunschweig, Germany; h.wehbe@tu-braunschweig.de (H.W.); s.hartwig@tu-braunschweig.de (S.H.); m.kandula@tu-braunschweig.de (M.W.K.)

\* Correspondence: lar.schmidt@tu-braunschweig.de

**Abstract:** Lithium metal exhibits strong adhesive properties and a highly reactive nature, which complicates conventional mechanical separation methods. Laser cutting, as a contactless process, is possible under a defined drying room atmosphere. However, it is a costly process and therefore not suitable for industrial usage. Consequently, the development of a cost-effective process gas is imperative for the future implementation of lithium metal. In this research, the laser cutting of 30 µm lithium copper composite foil is performed under different process gases (nitrogen and argon) and ambient atmospheres with different water contents to determine the ablation potential depended on the process gas. To assess the laser–material interaction, the impact of pulse repetition frequency and cutting velocity on the material behavior was investigated. To this end, the ablation behavior, the resulting cutting edges, and the electrochemical performance were thoroughly explored. The findings reveal a dependence of the ablation behavior on the water content in the ambient atmosphere, as well as a reduced energy input for a complete shot through when using an inert gas. The resulting cutting edges result in nearly similar outcomes with regard to the heat-affected zone. The electrochemical performance illustrates the influence of the laser process with different gases, taking into account the changed electrochemical impedance spectroscopy.



Academic Editor: Johan E. ten Elshof

Received: 8 April 2025

Revised: 13 May 2025

Accepted: 15 May 2025

Published: 15 May 2025

**Citation:** Schmidt, L.O.; Wehbe, H.; Hartwig, S.; Kandula, M.W.

Investigation of the Laser Material Interaction of Lithium Copper Foils Under Different Process Gases for All-Solid-State Batteries. *Batteries* **2025**, *11*, 195. <https://doi.org/10.3390/batteries11050195>

**Copyright:** © 2025 by the authors. Licensee MDPI, Basel, Switzerland. This article is an open access article distributed under the terms and conditions of the Creative Commons Attribution (CC BY) license (<https://creativecommons.org/licenses/by/4.0/>).

**Keywords:** lithium metal; laser application; lithium-ion batteries

## 1. Introduction

Lithium metal has been identified as a promising anode material for future battery systems, exhibiting a high specific capacity ( $3860 \text{ mAhg}^{-1}$ ), a low density ( $0.534 \text{ gcm}^{-3}$ ), and the lowest negative electrochemical potential ( $-3.04 \text{ V}$ ) [1]. However, the processing of this material poses significant challenges due to the strong adhesion and highly reactive nature of lithium as an alkali metal.

Conventional mechanical separation techniques, widely employed in the fabrication of battery electrodes, are incompatible with lithium metal due to the risk of abrasion of the cutting edge on the cutting die. Consequently, laser cutting, as a contactless separation process, emerges as a viable alternative [2], since laser applications are already employed for the processing of lithium metal in the field of ultrashort pulses for the reconditioning of lithium surfaces [3] and the structuring of electrodes [4]. Despite the wide range and suitability of laser applications in this context, there are still challenges with this method that need to be addressed. The high reactivity of lithium metal poses a dual challenge: the process must be carried out under specific conditions to prevent ignition from the thermal energy input, which could ignite the metal, and from reactions with the gas components

of the atmosphere. These reactions could lead to the formation of lithium nitride, lithium oxides, lithium hydroxides, and lithium carbonates on the lithium surface during the laser cutting process [5]. It is imperative to note that a drying room atmosphere with a water content below 5 ppm is instrumental in hindering both the reaction of lithium with the gas components and the ignition of the metal. However, the cost of such a drying room atmosphere is not conducive to its suitability for industrial applications. Consequently, an alternative process atmosphere is required to ensure consistent cutting edge quality and efficient electrochemistry. The selection of the process atmosphere is influenced by the resulting lithium compounds, as these exhibit varying bonding energies. In the context of laser cutting, these dependencies necessitate an alternative immediate energy input due to alterations in surface chemistry, which, in turn, give rise to a novel laser material interaction.

The reactions of lithium exhibit a strong dependence on the surrounding water content. At a water content of approximately 10 parts per million (under standard conditions), lithium reacts instantaneously with the components of the surrounding medium. Conversely, at lower water contents, the reaction rate slows significantly. At this point, lithium reacts preferentially with nitrogen to form lithium nitride. Conversely, as the water content increases, the reactivity of lithium with oxygen increases, resulting in reactions with lithium oxide or lithium hydroxide. The resulting lithium compounds exhibit varying binding energies, suggesting that disparate energy inputs are necessary to disaggregate the metal and that distinct ablation thresholds exist [5].

Research has already been conducted on laser cutting of lithium metal and the influence of the atmosphere on the cutting edge quality. However, the impact of dew point on cutting edges has been systematically examined only in the context of a pure 100  $\mu\text{m}$  lithium metal foil [2]. In the present study, lithium copper composite foils with a thin lithium layer of 20  $\mu\text{m}$  are utilized. The foils are cut under argon as an inert gas, under nitrogen as an active gas, and under atmospheres with water contents of <5 ppm or >5 ppm. The subsequent investigation will focus on the resulting ablation behavior, the heat-affected zone, and the electrochemical performance of the foils.

## 2. Materials and Methods

In this study, lithium copper composite foils consisting of a 20  $\mu\text{m}$  lithium layer deposited on a 10  $\mu\text{m}$  copper layer are utilized for this investigation (Goodfellow GmbH, Hamburg, Germany). Although laser cutting of lithium under varying dew points has already been investigated [2], those studies were conducted on pure lithium metal foils with a thickness of 100  $\mu\text{m}$  and without a copper backing. However, these layers are not applicable to future battery technologies, where lithium coatings typically range between ~30  $\mu\text{m}$  [6]. Furthermore, while Jansen et al. focused solely on the influence of dew point, the presented study expands the scope by also evaluating the effect of different process gases on the laser ablation behavior of this more application-relevant composite structure. The incorporation of a copper backing layer engenders substantial disparities in thermal and mechanical properties when compared to pure lithium foils. The high thermal conductivity of copper ( $400 \text{ W m}^{-1} \text{ K}^{-1}$ ) facilitates rapid head dissipation during laser processing, which has the potential to reduce the extent of the heat-affected zone (HAZ) and minimize thermal damage to the lithium layer [7].

Prior to the commencement of the experiment, the foils were stored under an argon atmosphere.

The laser system employed in this study is a pulsed nanosecond laser, as detailed in Table 1. It has been established that the utilization of ultrashort pulses results in optimal processing quality [8]. However, it should be noted that these laser systems attain lower ablation rates and possess significantly higher acquisition costs [9]. Consequently, nanosec-

ond laser systems are the preferred choice in industry and represent the state of the art in conventional lithium-ion battery production [4]. The velocity of 300 mm per second was selected as the maximum threshold in this study due to the available laser power. However, it is possible to upscale the results while maintaining the pulse overlap [4], which makes it possible to transfer these findings to more powerful systems.

**Table 1.** Laser system and investigated cutting parameters.

Nanosecond Laser System	
Model	G4 Pulsed Fiber Laser, SPI Lasers
Wavelength $\lambda/\text{nm}$	$1062 \pm 2$
Pulse duration $f/\text{s}$	$240 \times 10^{-9}$
Average power $P_{\text{AVG}}/\text{W}$	$72 \pm 2$
Spot diameter $d_{\text{spot}}/\mu\text{m}$	$74 \pm 3$
Frequencies $f/\text{kHz}$	70, 285, 490
Cutting velocities $v_c/\text{mm s}^{-1}$	50, 100, 150, 200, 250, 300

The laser system (see Table 1) is situated within a drying room atmosphere with a water content of less than 5 parts per million (ppm). Within the cutting system, a microenvironment was inundated with the respective process gas. The process gases utilized in this study included nitrogen (5.0 ppm, supplied by Westfalen AG, Münster, Germany) and argon (4.8 ppm, supplied by Westfalen AG). These gases were employed in atmospheres with water contents ranging from below 5 ppm to above 5 ppm.

To investigate the ablation behavior, the ablation depth was examined by increasing the number of pulses until a complete shot through was achieved. The ablation depth was examined with a confocal laser scanning microscope (Keyence GmbH, Neu-Isenburg, Germany).

To investigate the heat-affected zone, lithium copper foils were cut under varying laser parameters, including different frequencies and cutting velocities (see Table 1). The resulting heat-affected zone was determined by optical measurements of the thermal-stressed areas using a digital light microscope (Keyence GmbH, Neu-Isenburg, Germany).

In the context of the electrochemical performance, symmetrical half cells were constructed for the purpose of electrochemical impedance spectroscopy (EIS) [10]. In this study, lithium copper foils with a diameter of 18 mm were cut under either process gas or atmospheric conditions with varying water content. The cell housing was provided by PAT-Cell (EL-Cell, GmbH, Hamburg, Germany), and the single-use 220  $\mu\text{m}$  thick PP fiber separator and LiPF<sub>6</sub> + 2% VC + 10% FEC electrolyte were utilized as cell components. Although the present study concentrates on all-solid-state batteries (ASSBs), a liquid electrolyte was intentionally utilized to isolate and examine the effects of laser-induced modifications on the lithium metal surface. The utilization of a liquid electrolyte circumvents the prevalent challenges associated with solid-state electrolytes, including inadequate interfacial contact, substantial interfacial resistance, and mechanical instability [11–13]. This approach enables a targeted analysis of the surface chemistry, without interference from complex electrode–electrolyte interface phenomena. Moreover, given the absence of a consensus on a universally optimal solid-state electrolyte—whether sulfide-, oxide-, or polymer-based—that would be applicable to all systems, the surface-related findings presented here can be regarded as applicable to a wide range of ASSB systems [14]. Electrical impedance spectroscopy (EIS) was measured using the PAT-Tester-x-8 (EL-Cell, GmbH). The frequency range was from 10,000 Hz to 0.01 Hz, and the applied current was 0.366 mA.

### 3. Results and Discussion

#### 3.1. Drilling Experiment—Ablation Behavior

The drilling experiments were investigated to understand the laser–material interaction with regard to the ablation behavior. As illustrated in Figure 1, the ablation behavior of the lithium copper foils under investigation was examined for various process gases and water contents, as well as for different frequencies and pulse energies, respectively. It was observed that, at lower frequencies or with lower pulse energies the ablation behavior exhibited a reduced number of pulses required for a complete shot through when compared to higher frequencies or pulse energies. Furthermore, an increase in frequency to 285 kHz or 490 kHz led to an increase in the number of pulses required for a complete shot through. It is noteworthy that, as the frequency increases, the increase in ablation depth per pulse becomes more linear. This phenomenon is particularly evident in the context of thermally controlled ablations, where the accumulation of heat plays a pivotal role [15]. The investigation encompassed a range of process gases and water contents, with drilling under argon conditions demonstrating the minimum number of pulses required. Conversely, the synthetic air mixture with a water content >5 ppm necessitates the greatest number of pulses. The ablation behavior for the drying room atmosphere with a water content of 5 ppm and nitrogen exhibit a nearly equivalent range, considering the standard deviation. This observation can be attributed to the varying binding energies exhibited by the lithium compounds. The laser energy introduced in this process disrupts the lithium bonds, leading to the formation of a new bond with the surrounding gas components. Due to the temporal extent of the chemical reaction, which is measured in femtoseconds, bonds are broken, and new bonds are formed between each laser pulse.

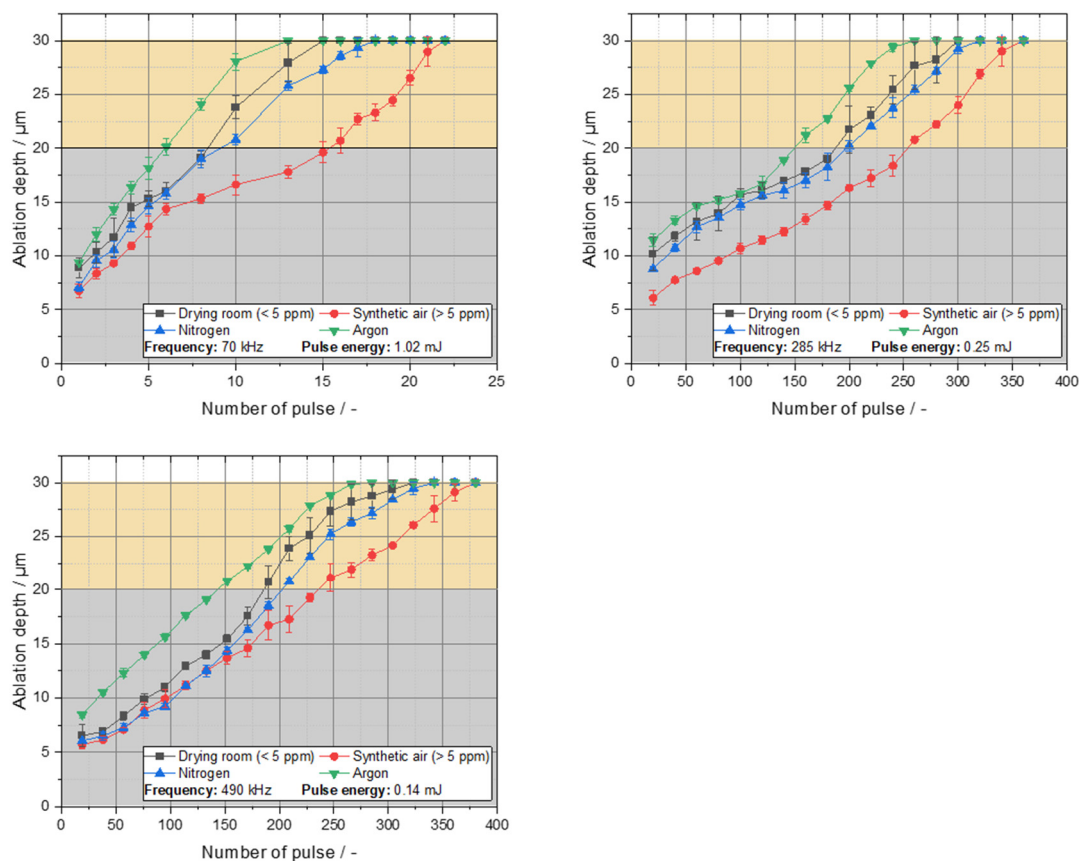


**Figure 1.** Ablation depth over number of pulses of the investigated lithium copper foils for different process gases, water contents and frequencies, obtained by drilling with Nd:YAG laser.

During the drilling process under nitrogen, this gas functions as a reactant, likely facilitating the formation of a lithium nitride bond. The synthetic air, characterized by a water content of less than 5 parts per million (ppm), is composed of the atmospheric air and, consequently, possesses an approximate nitrogen content of 80% [16]. The formation of lithium nitrides under these conditions is hypothesized to occur due to the selective binding of lithium with nitrogen in a dry atmosphere with a nitrogen content of <5 ppm. Consequently, the nitrogen and drying room gradient progress within a comparable range under analogous conditions.

However, drilling under synthetic air with a water content greater than 5 ppm leads to different ablation behaviors. The synthetic air mixture exhibits a substantially elevated water content compared to dry air. At higher water contents, lithium reacts preferentially with oxygen (or hydrogen) to form lithium oxide or lithium hydroxide, respectively. Consequently, the likelihood of the formation of lithium oxide and lithium hydroxide is increased. This is further supported by the binding energies of lithium oxide ( $179.53 \text{ kJg}^{-1}$ ) or lithium hydroxide ( $221.17 \text{ kJg}^{-1}$ ) to lithium nitride ( $153.19 \text{ kJg}^{-1}$ ), which are significantly higher than the binding energies of the aforementioned elements [5,17]. Consequently, a higher energy input is necessary to achieve a complete shot through, given the higher binding energies. Table 2 shows the results of an area EDS analysis.

**Table 2.** EDS measurement for lithium metal cut ( $\text{PRF} = 285 \text{ kHz}$ ,  $v_c = 300 \text{ mms}^{-1}$ ) under different process gases and atmospheres with different water content.

	Carbon	Nitrogen	Oxygen
Drying Room < 5 ppm	0.234781	0.47931	0.285909
Argon	0.264212	0.485916	0.249871
Nitrogen	0.155648	0.647169	0.197183
Synthetic Air > 5 ppm	0.239442	0.11258	0.6493

The EDS analysis of the cut electrodes reveals distinct differences in elemental composition depending on the surrounding atmosphere during cutting. In the context of drying room conditions and an argon atmosphere, the measured values demonstrate a high degree of similarity, suggesting that surface reactions are minimal. Conversely, electrodes that are cut under a nitrogen atmosphere exhibit the highest nitrogen content. The highest oxygen content is observed in samples processed in synthetical air with a water content > 5 ppm. The findings discussed herein are consistent with the previously discussed binding energies and align well with the results obtained from the drilling experiment.

The drilling process under argon exhibits two predominant effects on the ablation behavior. Initially, argon functions as a shielding gas, impeding the oxidation of lithium during the drilling process. Consequently, lithium itself becomes the sole potential reactant. While lithium–argon compounds have been observed, their formation necessitates elevated pressures and temperatures [18], which are presumably not present in this context. Consequently, the prevailing hypothesis suggests that the presence of lithium–argon compounds is improbable, and that the predominant compounds are likely dilithium compounds. These compounds exhibit the lowest binding energy of all lithium combinations, with a value of  $7.27 \text{ kJg}^{-1}$ , as reported in reference [19]. The minimal number of pulses required for a successful shot-through process lends further support to the presumed low binding energies. However, the observed discrepancy in the requisite number of pulses appears too insignificant in comparison to the other compounds, which exhibit substantially higher binding energies. Consequently, the secondary predominant effect appears to be plasma shielding. The plasma formation under argon could lead to shielding of the laser radiation, thereby reducing the energy coupling [20].

As illustrated in Figure 2, the ablation thresholds vary with both frequency and process gas. Generally, it can be observed that, under constant conditions, the process gases do not directly impact the fluence required for ablation. The ablation threshold for drilling at 70 kHz is  $2.5 \text{ Jcm}^{-2}$ , at 285 kHz it is  $12.2 \text{ Jcm}^{-2}$ , and for 490 kHz the necessary laser fluence is  $7.0 \text{ Jcm}^{-2}$ . Other studies have demonstrated that the ablation threshold for a  $50 \mu\text{m}$  lithium foil at a pulse duration of 261 ns and a frequency of 1 kHz was  $35.5 \text{ Jcm}^{-2}$  [4]. Consequently, the observed ablation thresholds appear to be within the expected range, as the ablation threshold generally decreases with higher frequencies [15]. However, this phenomenon was not observed in the present study. Furthermore, it has been demonstrated that the selection of process gases can indeed influence the ablation depth. This phenomenon has been previously documented by Elsied et al. in the context of aluminum and tungsten [21]. Notably, drilling under argon has been observed to result in a greater depth of drilling. This outcome is counterintuitive, as drilling under argon typically results in significant energy dissipation due to the plasma's energy absorption characteristics, leading to a substantial reduction in available energy for material removal [22]. However, it is important to note that these observations are primarily applicable to pure materials and do not extend to composite foils or reactive alkali metals. The underlying mechanism pertains to the prevention of oxide layer formation at the surface, which in turn weakens the lithium bonds. This effect, despite the attenuation of laser energy by plasma formation, ensures sufficient energy for achieving substantial ablation depths.

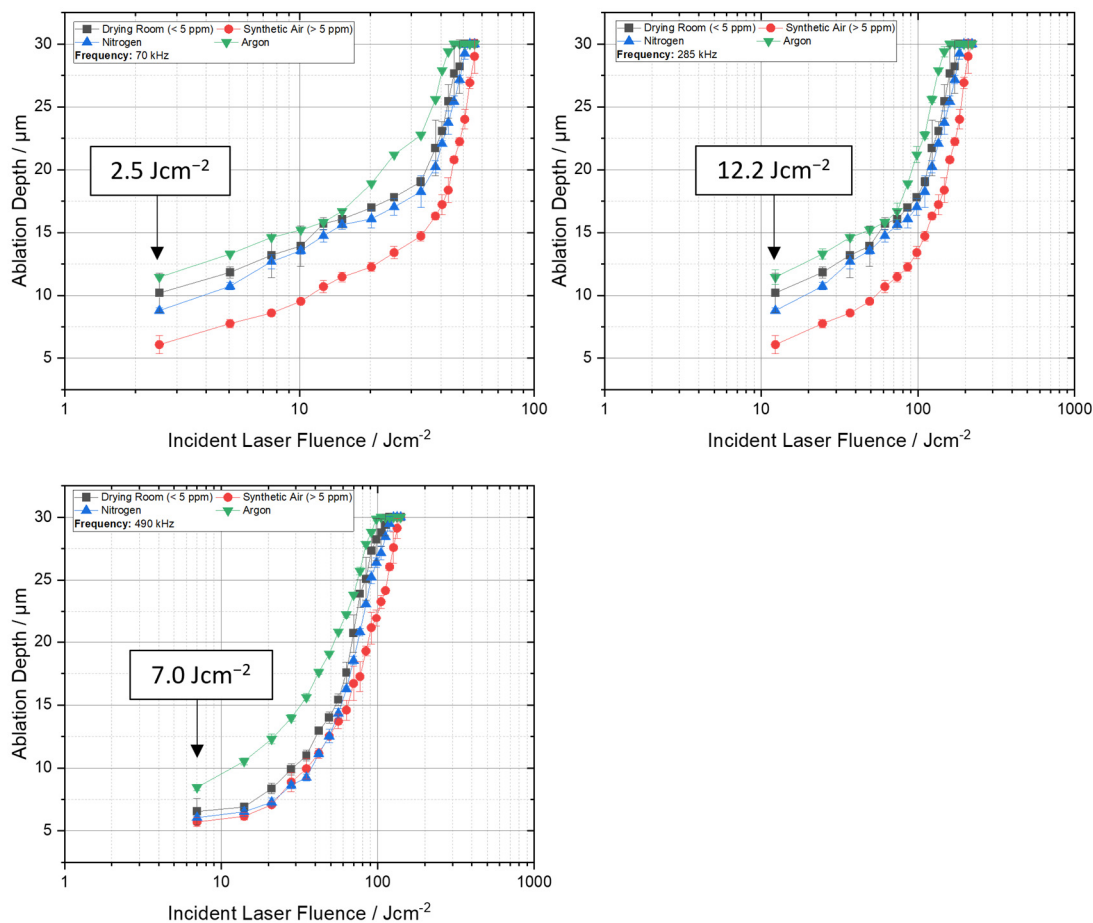


**Figure 2.** Dependence of the ablation depth on incident laser fluence for different pulse repetition frequencies of 70 kHz, 285 kHz and 490 kHz.

### 3.2. Cutting Experiment—Heat-Affected Zone

The term heat-affected zone (HAZ) is defined differently across various scientific and engineering disciplines. In the field of welding technology, the HAZ denotes the region adjacent to the weld that undergoes microstructural alterations due to thermal exposure. The assessment of these alterations frequently involves cross-sectional metallographic analysis [23,24]. In contrast, within the battery production, the HAZ is more frequently delineated based on visible surface modifications discernible from a top-down perspective. This approach is primarily adopted due to impracticality analysis in such delicate materials [1,25]. Nonetheless, the HAZ plays a critical role in battery applications, as it has measurable impact on the electrochemical performance of the cell. Changes in the surface morphology or chemistry of the HAZ have been demonstrated to exert a significant influence on interfacial resistance, SEI formation, and ionic transport [26]. Therefore, understanding and minimizing the HAZ is essential for ensuring consistent and efficient battery performance. Figure 3 illustrates the HAZ of the cut lithium copper foils at varying cutting velocities. A preliminary observation reveals a consistent trend across all diagrams: at constant cutting speeds, the HAZ increases with increasing frequencies. Conversely, the HAZ exhibits a decline at higher cutting velocities. This phenomenon can be attributed to the energy density, ED:

$$ED = \frac{P_{avg}}{V_c * d_{spot}} \left[ \frac{J}{mm^2} \right]$$

which is the quotient of the average power of the laser  $P_{avg}$ , and the cutting velocity  $V_c$  as well as the spot diameter  $d_{spot}$  [26]. In general, high cutting velocities reduce the line energy and lead to a reduction in the HAZ.

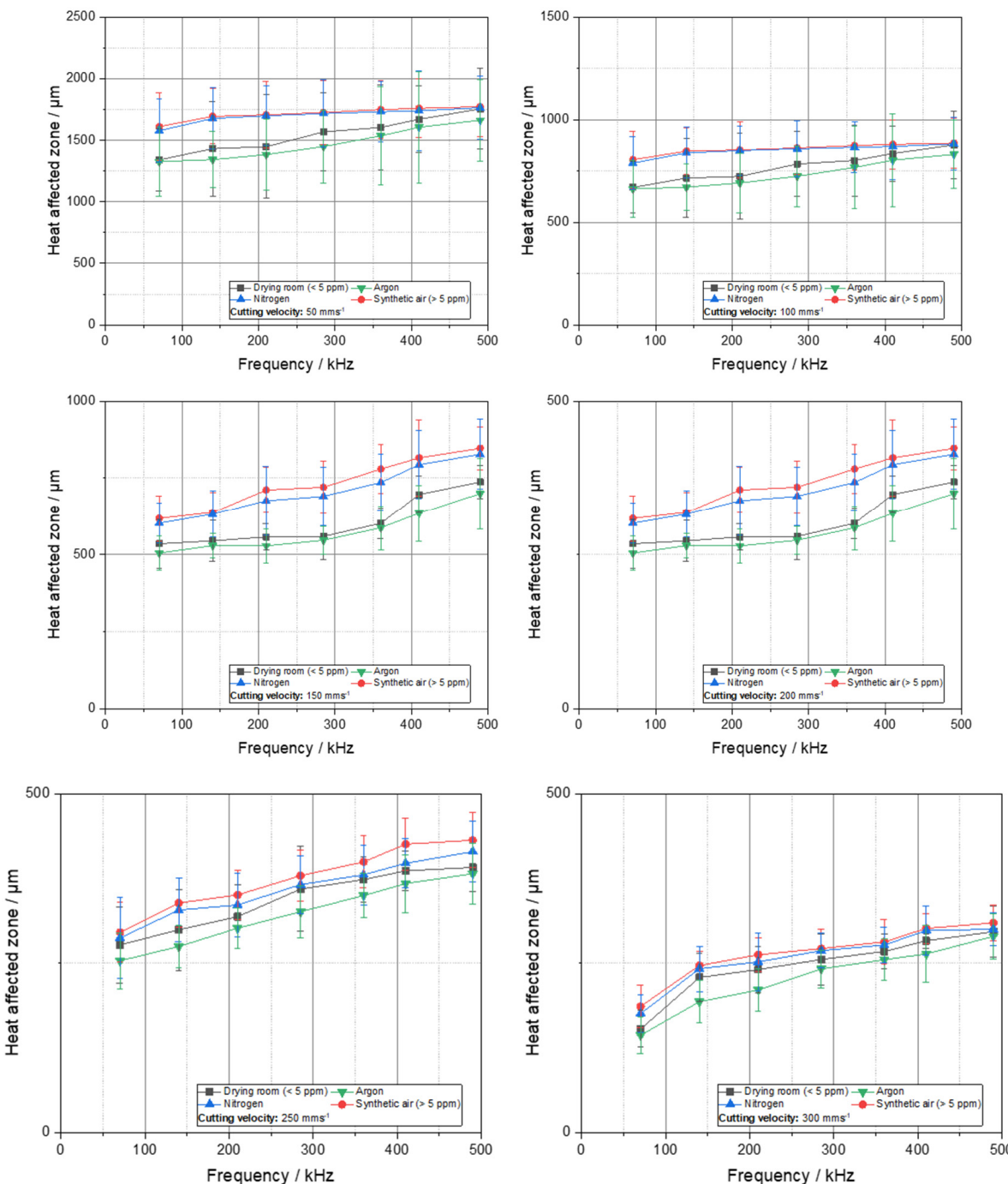
A consideration of the heat-affected zone (HAZ) in relation to the process gas or atmosphere, with varying water contents, reveals that the argon process yields the smallest average HAZ. However, when the standard deviation is taken into account, these values are found to be within a similar range. Consequently, a definitive differentiation among the various process gases is not possible. This observation aligns with prior findings in other materials where the process gas exhibited no direct influence on the length of the heat-affected zone [24]. It is noteworthy that a cutting velocity of  $50\text{ mms}^{-1}$  a high heat-affected zone of nearly  $1.5\text{ mm}$  is achieved. Conversely, at a substantially higher cutting velocity of  $300\text{ mms}^{-1}$ , the HAZ ranges from  $100$  to  $300\text{ }\mu\text{m}$ . In the context of battery production, this width of the HAZ is appropriate and will therefore lead to a further reduction in the HAZ at higher cutting velocities. Additionally, the range of the HAZ is attributable to the geometry selected, which in this instance is a circular blank. The necessity of a circular blank for cell cycling renders these shapes a subject of study in this context, aiming to quantify potential influences on electrochemistry. The conduction of heat within the metal during the cutting process is a primary factor contributing to the observed differences in thermal stress time for different geometries. Specifically, the cutting of a circular blank results in a longer thermal stress time for an area increment compared to a straight-line cut. Consequently, the heat-affected zone exhibits a substantial increase in size. The heat-affected zones resulting from cutting at  $300\text{ mm per minute}$  are illustrated in Figure 4. This cutting velocity was selected as it represented the highest attainable cutting rate within the present power range of the laser. It should be noted that faster cutting is possible with more powerful lasers, should a scale-up be desired.

Figure 4 illustrates the effects of process gases and atmospheres with varying water contents. For lower frequencies, it is evident that the laser cutting process is removing lithium from the copper substrate. As the frequency increases, the proportion of optically

visible copper decreases. This phenomenon can be attributed to the modification of pulse overlap, PO:

$$PO = \left( 1 - \frac{V_c}{PRF * d_{spot}} \right) * 100[\%]$$

which is the quotient of the cutting velocity  $v_c$ , the pulse repetition frequency PRF, as well as the spot diameter  $d_{spot}$  [2]. The pulse overlap increases with increasing frequency, by constant spot diameter and cutting velocity. Thus, the pulse overlap at 70 kHz is 96.22%, at 285 kHz it is 98.67%, and for 490 kHz it is 99.23%. With a smaller pulse overlap, the effects of accumulated heat decrease, so the introduced energy is no longer sufficient for complete ablation.



**Figure 3.** Heat-affected zone over frequency for the investigated process gases and different water contents by cutting under different cutting velocities (consider the different HAZ range).

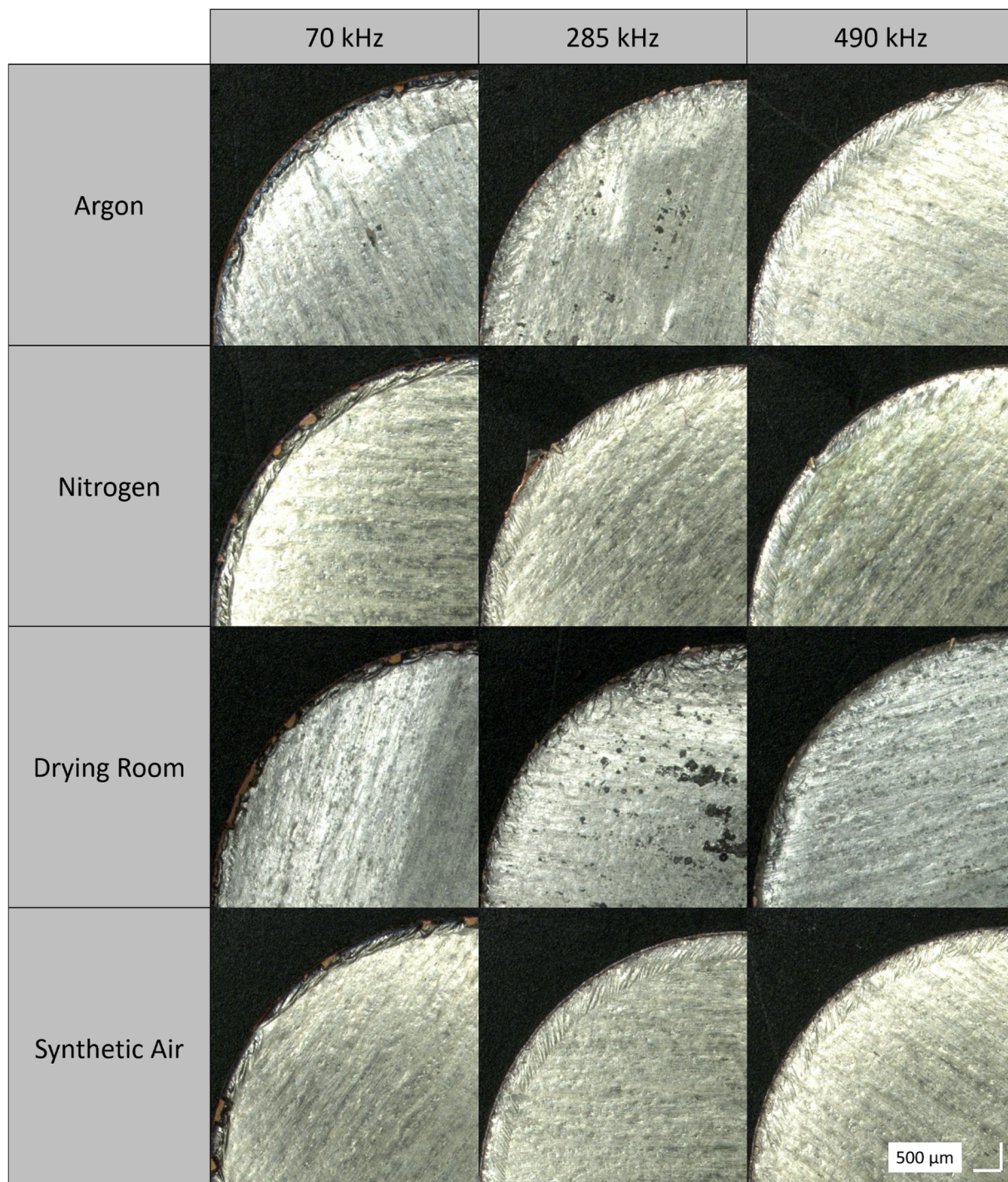


**Figure 4.** Light microscope images of the cutting edges, cut with a cutting velocity of  $300 \text{ mms}^{-1}$  at different frequencies (70 kHz, 285 kHz and 490 kHz) and process gases.

The drilling test results demonstrate that drilling under argon necessitates the least energy to achieve complete shoot through. These findings are corroborated by the present data. At 70 kHz, argon exhibits a reduced number of free copper spots, indicating that even at low pulse overlap, the energy input is sufficient to remove the material. Conversely, the energy input required for synthetic air is considerably higher, resulting in insufficient energy to remove lithium and copper, and the presence of residual copper spots. The disparities in the cutting edges become indiscernible at higher frequencies. The drilling experiment results indicate that the number of pulses required for a complete shoot through is nearly

similar at 285 kHz and 490 kHz. Furthermore, the pulse overlaps are more proximate at 285 kHz and 490 kHz than at 285 kHz and 70 kHz, thereby rendering the analogous cutting edge patterns contingent on the process gases more evident. Thus, for the evaluation of the heat-affected zone, it can be stated that there were no decisive differences with regard to the length of the heat-affected zone within the standard deviation; however, the appearance of the cutting edge differed depending on the process gas.

### 3.3. Electrochemical Characterization—Electrochemical Impedance Spectroscopy

As illustrated in Figure 5, the Nyquist plots of symmetric half cells of lithium copper foils are shown to be cut under various gases and atmospheres with different water contents. It is evident that only the first semicircle in the high and intermediate frequency range of the EIS measurement is taken into account, as this is the transition point between the anode and the electrolyte (referred to as RSEI resistance) [27]. This area is given particular attention in this study, as it is hypothesized that cutting under different media will alter the surface chemistry, leading to variations in SEI formation or ionic resistances, respectively. The nature and stability of the SEI, which forms spontaneously on the lithium surface, are contingent on the ambient water content and the specific lithium compounds generated during processing.

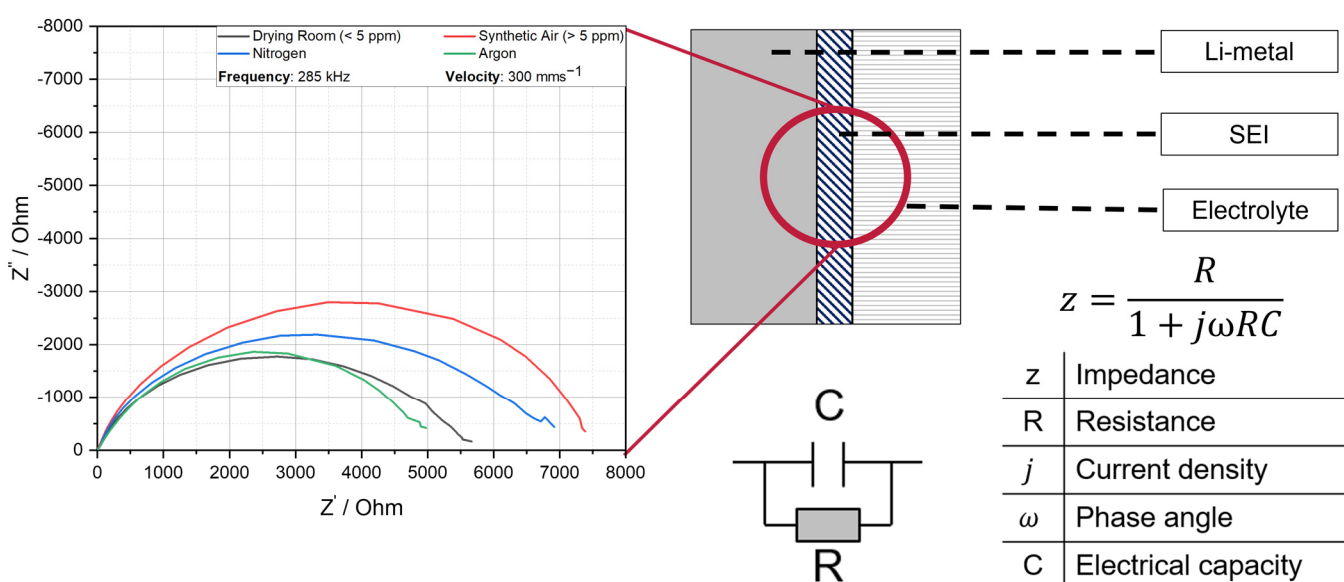


**Figure 5.** Electrochemical impedance spectroscopy of laser cut lithium copper foils ( $PR = 285$  kHz,  $v_c = 300$  mms $^{-1}$ ) under different process gases and atmospheres with different water contents.

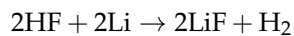
The phenomenon of low ionic impedance for the lithium, cut under drying room with a water content  $<5$  ppm and argon, can be attributed to the following chemical reaction, by considering the similar EDS values represented in Table 2. By cutting under atmospheres with a water content  $<5$  ppm, the reaction of the cut lithium metal surface with  $\text{LiPF}_6 + 2\% \text{ VC} + 10\% \text{ FEC}$  primarily leads to lithium fluoride (LiF) and polymerized vinylene carbonate (VD) species. These products contribute to the formation of a thin, homogenous, and stable SEI layer, which is crucial for efficient lithium-ion transport and the mechanical stability of the interface. A LiF-rich SEI is particularly advantageous due to its chemical inertness, high thermal stability, and electronic insulation properties, which collectively enhance passivation and suppress further electrolyte decomposition [28]. The use of a drying room and of argon promote the formation of a LiF-rich SEIs. This process

reduces undesired side reactions due to the absence of reactive species, and these findings are consistent with the EDS measurements presented in Table 2.

However, by cutting under an atmosphere with a water content >5 ppm, the highest ionic resistance is observed. Here, three distinct types have been identified as potential contributors to the formation of SEI: The presence of lithium oxides, lithium hydroxides, or water deposits on the surface due to the higher water content. With additional water, hydrolysis of LiPF<sub>6</sub> becomes significant, producing HF and POF<sub>3</sub>.

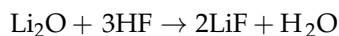


HF reacts aggressively with lithium, forming additional LiF but also generating H<sub>2</sub> gas,



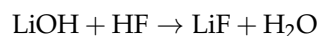
which can lead to porosity and mechanical inhomogeneity in the SEI. Furthermore, the presence of HF and its radicals has been shown to accelerate the polymerization of electrolyte additives such as FEC and VC, resulting in a thicker, less uniform SEI. This, in turn, has been demonstrated to impair interfacial stability and increase impedance [28].

Conversely, lithium oxide (Li<sub>2</sub>O) also reacts with HF to yield LiF and water.

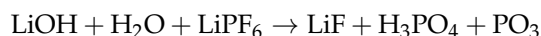


This pathway stabilizes the SEI through the formation of a LiF-enriched layer, while the released water may have limited detrimental effects depending on its concentration. Li<sub>2</sub>O contributes to the SEI's mechanical integrity and suppresses further parasitic reactions, making it a comparatively beneficial component [29].

Lithium hydroxide (LiOH) presents a significant challenge in this regard. When exposed to HF, the reaction product is LiF and water.

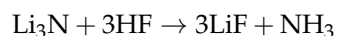


However, the presence of moisture has been shown to exacerbate SEI porosity and promote further degradation reactions, particularly under humid conditions. Furthermore, LiOH has been observed to react with LiPF<sub>6</sub>, resulting in the formation of POF<sub>3</sub> and H<sub>3</sub>PO<sub>4</sub>.



These reactions have been shown to compromise the uniformity of the SEI layer and to increase ionic resistance [30]. Thus, the highest ionic resistance is reached.

By cutting under nitrogen, lithium nitride is most likely to be formed. Lithium nitride has demonstrated potential in modifying the SEI favorably. The reaction of the compound with HF results in the generation of LiF and ammonia (NH<sub>3</sub>).



The presence of LiF contributes to the formation of a robust SEI, while NH<sub>3</sub> may undergo desorption or engage in secondary reactions with electrolyte decomposition products. It is noteworthy that Li<sub>3</sub>N has been demonstrated to enhance lithium-ion conductivity, thereby reducing interfacial resistance despite its comparatively higher resistance to pure lithium [31].

The results of the electrochemical impedance spectroscopy demonstrate that anodes cut under synthetic air (>5 ppm) exhibit both the highest displacement in the imaginary

axis ( $Z''$ ) and the longest elongation in the real axis ( $Z'$ ). Conversely, the impedance of the electrodes cut under synthetic air lies below the plot of the synthetic air. The impedance plots of the anodes cut under argon and those cut under dry room atmosphere (<5 ppm) demonstrate a tendency to align within a comparable range.

The use of argon as an inert atmosphere during the cutting process offers several advantages. It has been demonstrated that this method effectively protects the lithium surface from oxidation. Consequently, the surface of the cut lithium metal remains chemically relatively unchanged, resulting in minimal changes in electrochemical impedance. Furthermore, when the cutting process is conducted under a controlled atmosphere devoid of water vapor, with a water content of less than 5 parts per million (ppm), the electrochemical impedance spectroscopy (EIS) plot mirrors that of the argon-cutting anodes. This outcome is attributed to the inhibition or slowing of reactions with the surrounding components. This results in a surface chemistry of the lithium anode that is more or less similar, and consequently, a similar plot is observed. Conversely, cutting under nitrogen conditions leads to the formation of lithium nitrides. Given the measurement conditions, lithium nitrides generally exhibit a higher ionic resistance than lithium. Furthermore, it is expected that cutting under synthetic air with a high water content >5 ppm will result in inhomogeneous surface chemistry, comprising lithium nitrides, lithium oxides, and lithium hydroxides. This is likely to lead to significantly higher ionic resistance compared to the other process gases or atmospheres.

#### 4. Conclusions

The present study investigates the influence of different process gases and atmospheres with varying water contents on the ablation depth, the heat-affected zone, and the electrochemical performance. The experimental findings demonstrate a correlation between the process gas and the water content with the ablation behavior. It was observed that atmospheres with a water content greater than 5 ppm necessitated a higher number of laser pulses for all frequencies examined. Conversely, nitrogen atmospheres with a low water content (less than 5 ppm) exhibited nearly similar ablation behavior, attributed to the gas component distribution of the dry atmosphere, which contains approximately 80% nitrogen. The cutting process under argon can be influenced by two primary factors. Argon, being an inert gas, prevents the oxidation of lithium, thereby primarily targeting lithium bonds for cleavage. Additionally, the presence of plasma shielding significantly reduces the amount of energy introduced. Consequently, a conspicuously defined hole structure is formed at elevated pulse energies.

The influence of process gases and water content is negligible within the heat-affected zone. The zone is primarily influenced by the frequency and the cutting velocity. Notably, irrespective of the process gases employed, the heat-affected zones exhibit a comparable range within the standard deviation. For the electrochemical impedance spectroscopy, the influence of the process gases in terms of ionic resistance are exposed. The lowest ionic resistance is found under gases or atmospheres, which presumably does not lead to any surface change. In reactive gases and atmospheres with high water contents, which accelerate the reaction of the lithium, a significantly higher ionic resistance is determined.

In consideration of the aforementioned data, it can be posited that the implementation of argon as a cutting process may result in a reduction in the requisite energy input. This reduction may, in turn, lead to a diminished heat-affected zone and an electrochemical performance that is analogous to that of a conventional drying room reference. Consequently, argon emerges as a promising alternative as a process gas for the lithium metal processing in future all-solid-state batteries.

Subsequent investigations should focus on drilling and cutting under helium as a process gas. According to the current state of the art, helium is expected to yield significant improvements in terms of ablation depth per pulse and the absence of reaction of the reactive lithium surface with the surrounding medium [22,32].

**Author Contributions:** Conceptualization, L.O.S. and H.W.; methodology, L.O.S.; software, L.O.S.; validation, L.O.S.; formal analysis, L.O.S.; investigation, L.O.S., resources, M.W.K.; data curation, L.O.S.; writing—original draft preparation, L.O.S.; writing—review and editing, H.W., S.H. and M.W.K.; visualization, L.O.S.; supervision, M.W.K. All authors have read and agreed to the published version of the manuscript.

**Funding:** This research received no external funding.

**Data Availability Statement:** The original contributions presented in this study are included in the article, and further inquiries can be directed to the corresponding author.

**Conflicts of Interest:** The authors declare no conflicts of interest.

## References

1. Schmidt, L.O. Laserstrahlschneiden von Lithium-Metall Folien für den Gebrauch in All-Solid-State Batterie Systemen. In 4. Symposium Materialtechnik, *Fortschrittsberichte der Materialforschung und Werkstofftechnik/Bulletin of Materials Research and Engineering*; 4. Symposium Materialtechnik, Clausthal, 25.02–26.02.; Materialtechnik, C.Z.F., Ed.; Shaker Verlag: Düren, Germany, 2021; pp. 521–531, ISBN 978-3-8440-8021-6.
2. Jansen, T.; Blass, D.; Hartwig, S.; Dilger, K. Processing of Advanced Battery Materials—Laser Cutting of Pure Lithium Metal Foils. *Batteries* **2018**, *4*, 37. [[CrossRef](#)]
3. Kriegler, J.; Ballmes, H.; Dib, S.; Demir, A.G.; Hille, L.; Liang, Y.; Wach, L.; Weinmann, S.; Keilhofer, J.; Kim, K.J.; et al. Surface Reconditioning of Lithium Metal Electrodes by Laser Treatment for the Industrial Production of Enhanced Lithium Metal Batteries. *Adv. Funct. Mater.* **2024**, *34*, 2313766. [[CrossRef](#)]
4. Kriegler, J.; Nguyen, T.M.D.; Tomcic, L.; Hille, L.; Grabmann, S.; Jaimez-Farnham, E.I.; Zaeh, M.F. Processing of Lithium Metal for the Production of Post-Lithium-Ion Batteries Using a Pulsed Nanosecond Fiber Laser. *SSRN J.* **2022**. [[CrossRef](#)]
5. Jeppson, D.W.; Ballif, J.L.; Yuan, W.W.; Chou, B.E.; Hanford Engineering Development Lab. Lithium Literature Review: Lithium’s Properties and Interactions. 1978. Available online: <https://inis.iaea.org/records/0s4x9-bx611> (accessed on 3 May 2025).
6. Schönherr, K.; Schumm, B.; Hippauf, F.; Lissy, R.; Althues, H.; Leyens, C.; Kaskel, S. Liquid lithium metal processing into ultrathin metal anodes for solid state batteries. *Chem. Eng. J. Adv.* **2022**, *9*, 100218. [[CrossRef](#)]
7. Wang, J.; Cao, L.; Li, S.; Xu, J.; Xiao, R.; Huang, T. Effect of Laser-Textured Cu Foil with Deep Ablation on Si Anode Performance in Li-Ion Batteries. *Nanomaterials* **2023**, *13*, 2534. [[CrossRef](#)]
8. Leitz, K.-H.; Redlingshöfer, B.; Reg, Y.; Otto, A.; Schmidt, M. Metal Ablation with Short and Ultrashort Laser Pulses. *Phys. Procedia* **2011**, *12*, 230–238. [[CrossRef](#)]
9. Chen, X.; Liu, X. Short pulsed laser machining: How short is short enough? *J. Laser Appl.* **1999**, *11*, 268–272. [[CrossRef](#)]
10. Momma, T.; Yokoshima, T.; Nara, H.; Gima, Y.; Osaka, T. Distinction of impedance responses of Li-ion batteries for individual electrodes using symmetric cells. *Electrochim. Acta* **2014**, *131*, 195–201. [[CrossRef](#)]
11. Famprikis, T.; Canepa, P.; Dawson, J.A.; Islam, M.S.; Masquelier, C. Fundamentals of inorganic solid-state electrolytes for batteries. *Nat. Mater.* **2019**, *18*, 1278–1291. [[CrossRef](#)]
12. Koerver, R.; Zhang, W.; de Biasi, L.; Schweidler, S.; Kondrakov, A.O.; Kolling, S.; Brezesinski, T.; Hartmann, P.; Zeier, W.G.; Janek, J. Chemo-mechanical expansion of lithium electrode materials—on the route to mechanically optimized all-solid-state batteries. *Energy Environ. Sci.* **2018**, *11*, 2142–2158. [[CrossRef](#)]
13. Krauskopf, T.; Hartmann, H.; Zeier, W.G.; Janek, J. Toward a Fundamental Understanding of the Lithium Metal Anode in Solid-State Batteries—An Electrochemo-Mechanical Study on the Garnet-Type Solid Electrolyte Li<sub>6.25</sub>Al<sub>0.25</sub>La<sub>3</sub>Zr<sub>2</sub>O<sub>12</sub>. *ACS Appl. Mater. Interfaces* **2019**, *11*, 14463–14477. [[CrossRef](#)] [[PubMed](#)]
14. Sun, C.; Liu, J.; Gong, Y.; Wilkinson, D.P.; Zhang, J. Recent advances in all-solid-state rechargeable lithium batteries. *Nano Energy* **2017**, *33*, 363–386. [[CrossRef](#)]
15. Brygo, F.; Dutouquet, C.; Le Guern, F.; Oltra, R.; Semerok, A.; Weulersse, J.M. Laser fluence, repetition rate and pulse duration effects on paint ablation. *Appl. Surf. Sci.* **2006**, *252*, 2131–2138. [[CrossRef](#)]
16. Berner, E.K.; Berner, R.A. *Global Environment Water, Air, and Geochemical Cycles*; Princeton University Press: Princeton, NJ, USA, 2012; ISBN 978-0-691-13678-3.

17. Moulder, J.F.; Stickle, W.F.; Sobol, P.E.; Bomben, K.D. *Handbook of X-Ray Photoelectron Spectroscopy: A Reference Book of Standard Spectra for Identification and Interpretation of XPS Data*; Physical Electronics, Inc.: Chanhassen, MN, USA, 1995.
18. Li, X.; Hermann, A.; Peng, F.; Lv, J.; Wang, Y.; Wang, H.; Ma, Y. Stable Lithium Argon compounds under high pressure. *Sci. Rep.* **2015**, *5*, 16675. [[CrossRef](#)]
19. Hornby, M.; Peach, J. *Chemical Bonding*; Reprinted; Oxford University Press: Oxford, UK, 1995; ISBN 0198556942.
20. Chaudhary, K.; Rizvi, S.Z.H.; Ali, J. Laser-Induced Plasma and its Applications. In *Plasma Science and Technology—Progress in Physical States and Chemical Reactions*; Mieno, T., Ed.; InTech: Rijeka, Croatia, 2016; ISBN 978-953-51-2280-7.
21. Elsied, A.M.; Dieffenbach, P.C.; Diwakar, P.K.; Hassanein, A. Nanosecond laser-metal ablation at different ambient conditions. *Spectrochim. Acta Part B At. Spectrosc.* **2018**, *143*, 26–31. [[CrossRef](#)]
22. Vadillo, J.M.; Fernández Romero, J.M.; Rodríguez, C.; Laserna, J.J. Effect of plasma shielding on laser ablation rate of pure metals at reduced pressure. *Surf. Interface Anal.* **1999**, *27*, 1009–1015. [[CrossRef](#)]
23. Huang, C.A.; Wang, T.H.; Lee, C.H.; Han, W.C. A study of the heat-affected zone (HAZ) of an Inconel 718 sheet welded with electron-beam welding (EBW). *Mater. Sci. Eng. A* **2005**, *398*, 275–281. [[CrossRef](#)]
24. Marimuthu, S.; Dunleavy, J.; Liu, Y.; Antar, M.; Smith, B. Laser cutting of aluminium-alumina metal matrix composite. *Opt. Laser Technol.* **2019**, *117*, 251–259. [[CrossRef](#)]
25. Angeloni, C.; Magrini, C.; Liverani, E.; Fortunato, A. The effect of process parameters on the high-speed cut quality of Li-ion electrodes using a single mode continuous fiber laser. *Opt. Laser Technol.* **2025**, *189*, 113119. [[CrossRef](#)]
26. Jansen, T.; Kandula, M.; Hartwig, S.; Hoffmann, L.; Haselrieder, W.; Dilger, K. Influence of Laser-Generated Cutting Edges on the Electrical Performance of Large Lithium-Ion Pouch Cells. *Batteries* **2019**, *5*, 73. [[CrossRef](#)]
27. Choi, W.; Shin, H.-C.; Kim, J.M.; Choi, J.-Y.; Yoon, W.-S. Modeling and Applications of Electrochemical Impedance Spectroscopy (EIS) for Lithium-ion Batteries. *J. Electrochem. Sci. Technol.* **2020**, *11*, 1–13. [[CrossRef](#)]
28. Ha, Y.; Stetson, C.; Harvey, S.P.; Teeter, G.; Tremolet de Villers, B.J.; Jiang, C.-S.; Schnabel, M.; Stradins, P.; Burrell, A.; Han, S.-D. Effect of Water Concentration in LiPF<sub>6</sub>-Based Electrolytes on the Formation, Evolution, and Properties of the Solid Electrolyte Interphase on Si Anodes. *ACS Appl. Mater. Interfaces* **2020**, *12*, 49563–49573. [[CrossRef](#)] [[PubMed](#)]
29. Guo, R.; Gallant, B.M. Li<sub>2</sub>O Solid Electrolyte Interphase: Probing Transport Properties at the Chemical Potential of Lithium. *Chem. Mater.* **2020**, *32*, 5525–5533. [[CrossRef](#)]
30. Di Muzio, S.; Paolone, A.; Brutti, S. Thermodynamics of the Hydrolysis of Lithium Salts: Pathways to the Precipitation of Inorganic SEI Components in Li-Ion Batteries. *J. Electrochem. Soc.* **2021**, *168*, 100514. [[CrossRef](#)]
31. Wang, Q.; Wu, M.; Xu, Y.; Li, C.; Rong, Y.; Liao, Y.; Gao, M.; Zhang, X.; Chen, W.; Lu, J. In situ high-quality LiF/Li<sub>3</sub>N inorganic and phenyl-based organic solid electrolyte interphases for advanced lithium–oxygen batteries. *Carbon Energy* **2024**, *6*, e576. [[CrossRef](#)]
32. Perrie, W.; Gill, M.; Robinson, G.; Fox, P.; O'Neill, W. Femtosecond laser micro-structuring of aluminium under helium. *Appl. Surf. Sci.* **2004**, *230*, 50–59. [[CrossRef](#)]

**Disclaimer/Publisher’s Note:** The statements, opinions and data contained in all publications are solely those of the individual author(s) and contributor(s) and not of MDPI and/or the editor(s). MDPI and/or the editor(s) disclaim responsibility for any injury to people or property resulting from any ideas, methods, instructions or products referred to in the content.